Temperature Dependence of Reconfigurable Bandstop Filters Using Vanadium Dioxide Switches

Andrei A. Muller, Matteo Cavalieri, Adrian M. Ionescu

NanoLab, École Polytechnique Fedérale de Lausanne (EPFL), 1015 Lausanne, Switzerland

Author to whom correspondence should be addressed: andrei.muller@epfl.ch

ABSTRACT

In this letter we report and investigate the temperature dependency of various radio frequency (RF) parameters for a fabricated reconfigurable bandstop filter with vanadium dioxide (VO_2) switches measured up to 55 GHz. Here the insulator to metal (ITM) and metal to insulator transition (MIT) hysteresis of the VO_2 thin film influence on the RF characteristics of the filters is analyzed from 25 °C and 120 °C in heating and cooling. The resonance frequency and maximum insertion loss (IL) stability and sensitivity with temperature variations are explored. It is noticed that increasing the temperature with 50 °C from 25 °C (or decreasing it with 50 °C from 120 °C) will result in a less than 1% fractional frequency shift in respect to the off and on resonance frequencies. The sharp DC conductivity levels variations of the VO_2 thin film around the transition temperatures translate into sharp effects on the resonance characteristics of the filters. On the contrary, the maximum IL levels are less sensitive to the DC films sharp conductivity changes around the VO_2 transition temperature. A unique behavior is reported when successively heating-up and cooling-down, over and below, respectively, the transition temperature of VO_2: the fabricated filter exhibits completely different resonance frequencies. This suggests that in the temperature dependence of VO_2 RF design, the practical use of

reconfigurable RF functions have to take into account the history of thermal effects and increase or decrease of the device temperature when crossing the IMT/MIT transition point.

The phase-change material, vanadium dioxide (VO_2) exhibits a monoclinic crystal structure and behaves like an insulator below its insulating-to-metal transition temperature (T_{ITM}), which is around 68 °C in bulk VO_2[1-6]. Above this temperature the monoclinic crystal structure changes to tetragonal crystal structure. Conversely, a reversible Metal-to Insulator transition occurs at (T_{MIT}) a bit below 68 °C for bulk VO_2 when temperature is decreased. Furthermore, dimensional scaling applies, and the nature of the phase transition is additionally conserved in VO_2 thin films and ultra-thin films[6-7]. Unlike in single crystalline forms of VO_2 where both phase transitions occur around 68 °C and exhibit narrow hysteresis, in thin films the critical temperature (defined as the average between T_{ITM} and T_{MIT} i.e $T_c = (T_{ITM} + T_{MIT})/2$, the width of the hysteresis loop, and the amplitude of the transition depend strongly on the film morphology, doping and deposition substrate[7-8]. Due to the ultrafast transition, the switching between the insulating and metallic phases can occur very quickly, (in the order of a few phonon oscillations) and its relative closeness to room temperature, vanadium dioxide has raised tremendous interest in both fundamental research and a variety of applications in electronics. VO_2 has been used as a switching element in the infra-red frequency bands[9-11], THz regions[12-15] while recently too in the RF frequency bands[5,16]. VO_2 RF switches[16] can operate under a lower transition temperature with reduced power consumption, compared with other thermally triggered switches, particularly unlike most of the other RF switches based on diodes[17-20] or micro-electro-mechanical systems (MEMS) [21-24], the device structure and fabrication of VO_2 switches can be much simplified. VO_2 switches with small size and high linearity increased their attractiveness for the RF community too.

A variety of reconfigurable RF devices using VO_2 switches such as antennas[25], inductors[26], filters[27-30] have been recently reported. Their performance however is very much dependent on the VO_2 thin film depositions and conductivity levels in the insulating state (off state) and conductive state (on state). The thin films conductivity levels reach hundreds of thousands of

Siemens (S) above T_{IMT} when deposited on sapphire, while mostly just tenths of thousands of S when deposited on cheap CMOS Si substrates[26-30], hindering the on state behavior of the devices. In the off state on the other hand, the dielectric behavior and non-zero DC conductivity levels of the thin films are also affecting the RF performances.

Here, we report a reconfigurable bandstop filter using VO_2 switches on a CMOS compatible Si substrate exhibiting a wider tuning range with respect to all K, Ka or V band experimentally bandstop filters reported employing VO_2 switches[27-30]. The tuning range of the filter defined as $t(\%)= |f_{max}-f_{min}|/f_{max}$ where f_{max} and f_{min} represent the resonance frequencies of the filter at 25 °C and 120 °C respectively is here of 34% improving the tuning ranges reported in [27, 29-30] without deteriorating the attenuation levels. Further, unlike most studies which analyze the RF components behavior only at two temperatures[25-30], here we perform a series of measurements at a variety of temperatures on both DC films characteristics and on the RF parameters of the filters. The stability of the RF performances with temperature is extracted and the correspondence between the DC thin film temperature sensitivity and RF performance of the filters is analyzed.

The filters were fabricated using the same methodology as in standard microelectronic processes starting with a high-resistivity (10000 Ω·cm) 525 μm thick silicon substrate. A 300 nm thick amorphous silicon layer[31-33] was firstly deposited, then the substrate was passivated with 500 nm SiO_2 deposited by sputtering. The amorphous silicon layer was deposited using low-pressure chemical vapor deposition. The rationale for adding this layer is mainly related to the decrease the RF conductive losses associated to the Si-SiO_2 layer interface[31-33]. A 140 nm thin VO_2 film and was deposited at 400 °C in oxygen atmosphere by a Pulsed Laser Deposition (PLD) system using a V_2O_5 target and then annealed at 475 °C in the same system for 10 min. The film was then patterned using standard photolithography followed by dry etching. A Cr (20 nm)/Al (400 nm) bi-layer was deposited to contact the patterned VO_2 film.

This thin contact layer allowed for the realization of 1.3 µm gaps between the contact pads. Additionally, a 2.4µm-thick Al layer was deposited on top of these contact metal by conventional lift-off methods to create the final coplanar waveguide elements.

Fig. 1 (a) shows the filter schematic while Fig.1 (b) presents a cross sectional schematic of the switch. The angle θ represents the angle of an additional gap in a classical split ring topology[30], in respect to the common outer ring gap, here θ being at 5 o'clock unlike 3 o' clock in[30] (considering 12 o'clock where the classical outer gap lies). The classical split ring filter can be modeled by a total capacitance, (C) (corresponding to the inter-ring and gap capacitances), in addition to an inductance, (L), taken as the average inductance of the two rings[34]. The resonance frequency *fr* is then simply given as $1/(2\pi LC)$. In the fabricated filter the additional gap at 5 o'clock generates an additional series capacitance decreasing the overall capacitance of the split rings. On the other hand the gap position on the outer ring influences the total inductance value, as it approaches 6 o' clock, the active inductive part decreasing, this having a supplementary effect in shifting upwards the resonance frequency. Fig. 1 (c) shows the electric field at resonance simulated with HFSS for one of the upper left split ring in Fig. (1) (a).

Fig. 2 (a) presents the switch photo and Fig 2 (b) the surface of the VO_2 thin film used, where the grains can be observed.

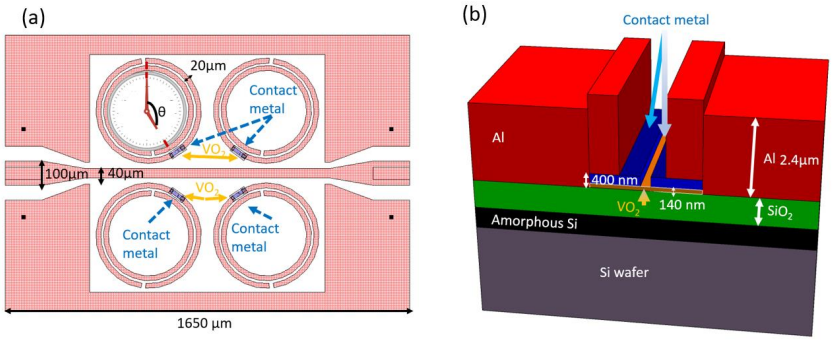

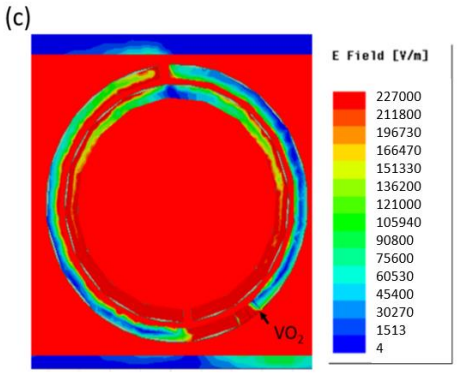

FIG. 1. (a) Schematic of the filter (b) Cross-sectional schematic of the switching elements. (c) Electric field at resonance in the left right split ring with a VO_2 filled gap.

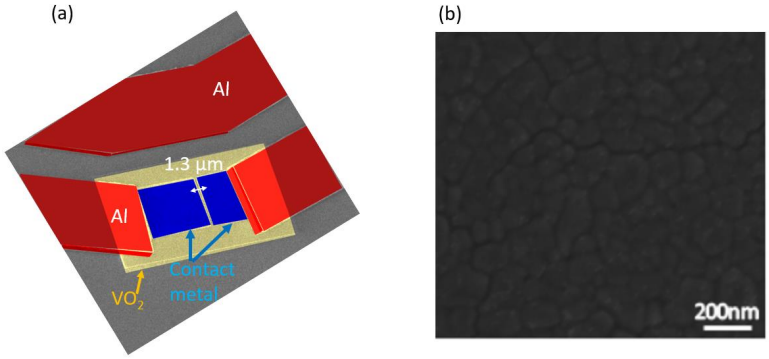

FIG. 2. (a) SEM photo with tuned colors of the switch (b) Surface photo of the VO_2 thin film with visible grains.

The filter RF performances are initially tested only at two different temperature values, as in most RF devices including VO_2 switches[5,25-30]. The tests are performed using an Anritsu vector network analyzer (VNA) with a heating stage below the sample in order to control its temperature. Figure 3 (a) shows the filter performances in terms of S_{21} (dB)- the filter exhibiting a resonance frequency of 45.64 GHz in off state (here at room temperature-25 °C)

and at 29.93 GHz in the on state (here at 120 °C). The maximum insertion loss (IL) at the off/on resonances are of 18.29 dB and 14.02 dB. The results improve in terms of reconfigurability the previous results including VO_2 switches for similar frequency bands exhibiting here a tuning range $t = |f_{max}-f_{min}|/f_{max} = 34$ %. A comparison in respect to previous works is displayed in Table 1, presenting the improvement with respect to our previous works[29-30] in respect to the tuning range.

Table I. RF filter performances using VO_2 switches at room temperature and at a temperature above T_{ITM} in heating up.

References	27	29	30	this work
Tuning range (%)	12%	19%	23%	34%
Maximum IL (dB)	16 and 18	12.8 and 18	14.10 and 18	14.02 and 18.29
Resonance frequencies (GHz)	19.8 and 22.5	28 and 34	29.74 and 38.70	29.93 and 45.64

Unlike most RF devices reported including VO_2 switches whose performances are only validated in on/off cases[5, 25-30], here we go further with the tests in order to understand how the heat influence on the VO_2 thin film alters the overall RF performances of the devices. First, the VO_2 thin film DC conductivity is assessed using four probe measurements and the results are presented in Fig. 3 (b). The on state conductivity levels are just below 50,000 S/m while the off state values are around 30 S/m- the results are in the same trend as other depositions on SiO_2/Si wafers[29,30], the conductivity of the VO_2 being considerably affected by substrate lattice mismatches, grain size and deposition parameters[7,8,30]. Then, we perform VNA measurements at 25 °C, 50 °C, 60 °C, 66 °C, 70 °C, 75 °C, 80 °C, 83 °C, 86 °C, 90 °C, 100 °C, 120 °C in heating up and cooling down and get the results presented in Fig. 3(c) and Fig. 3(d).

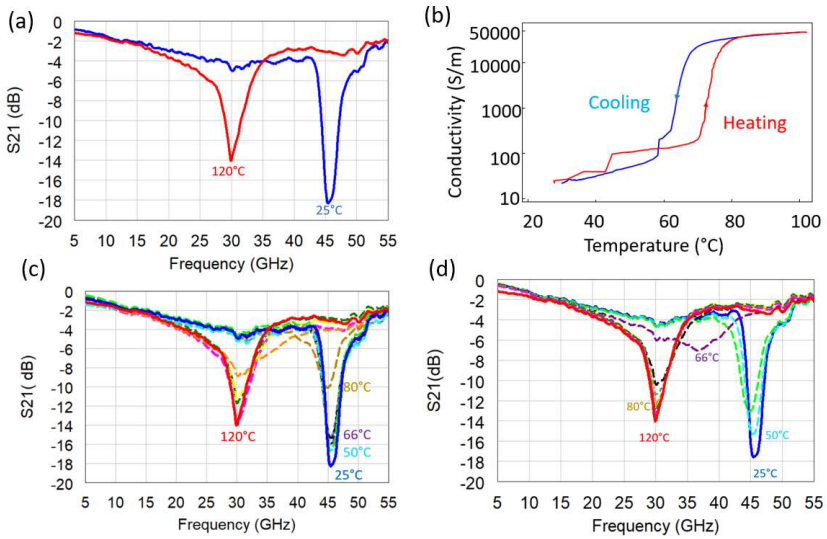

FIG. 3 (a) Filter on/off S21 (dB) parameter, (b) VO_2 thin film conductivity levels in heating and cooling. (c) S21(dB) parameter of the filter at 25 °C, 50 °C, 60 °C, 66 °C, 70 °C, 75 °C, 80 °C, 83 °C, 86 °C, 90 °C, 100 °C, 120 °C in heating (d) S21(dB) parameter in cooling.

From an RF point of view, one of the important features when it comes to a resonator is its temperature stability with respect to its resonance frequency and maximum insertion loss (IL) at the resonance frequency. In order to grasp this influence Fig 3 (c) and (d) results are arithmetically manipulated in Fig. 4 and Fig. 5 for understanding the resonance frequency (f_r) evolution with temperature change first and then the maximum IL at resonance.

Fig 4 (a) shows the variation of the resonance frequency once temperature is increased in respect to the off state and when temperature is decreased in respect to the on state. The graph illustrates little changes in heating up to 80 °C (and thus for a temperature variation of 55 °C) and also little changes when temperature decreases up to 70 °C from 120 °C. In Fig. 4 (b) we express this variation in terms of fractional frequency shift in respect to the off/on resonance

frequencies $\Delta f/f_{off}$ in heating and $\Delta f/f_{on}$ in cooling, where $\Delta f = f_r - f_{off}$ in heating and $\Delta f = f_r - f_{on}$ in cooling.

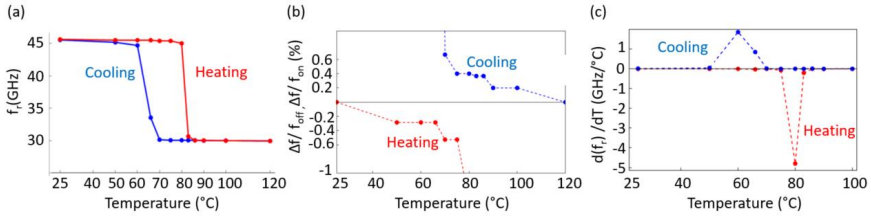

FIG. 4 In heating up and cooling down (a) Resonance frequency variation with temperature (b) fractional frequency shift in respect to the on and off resonance frequencies, (c) Derivatives of the resonance frequency variation in respect to temperature variation.

We may see a fractional frequency shift below 0.6 % in heating-up from room temperature to 75 °C and cooling down from 120 °C to 70 °C, overall observing that in order to keep the frequency stable with less than 0.6% variations one afford an increase of temperature to up to 75 °C, and while in cooling down a decrease up to 70 °C. Fig. 4 (c) shows the speed of the resonance frequency change in heating up and cooling down presenting a relative sharp transition around T_{ITM} and T_{IMT} of the VO_2 thin film.

Fig. 5 on the other hand exploits the attenuation changes with temperature increase and decrease expressed here in terms of maximum insertion loss (max IL). Fig. 5 (a) displays clearly how the maximum attenuation levels are deeply affected by the temperature changes. Fig 5 (b) illustrates the evolution of the fractional maximum insertion loss at resonance frequency variation with respect to the maximum levels in on and off states (where $\Delta IL(dB) = IL(f_r) - IL(f_{off})$ in heating and $\Delta IL(dB) = IL(f_r) - IL(f_{on})$ in cooling). One may notice a change of 17 % increasing the temperature from 25 °C to 75 °C. The same is observed in cooling when the temperature is decreased to 75 °C. Fig 5 (c) displays the resonance frequency change in heating and cooling

showing a relative far less sharp transition around T_{ITM} and T_{IMT} of the VO_2 thin film than in the case of the resonance frequency.

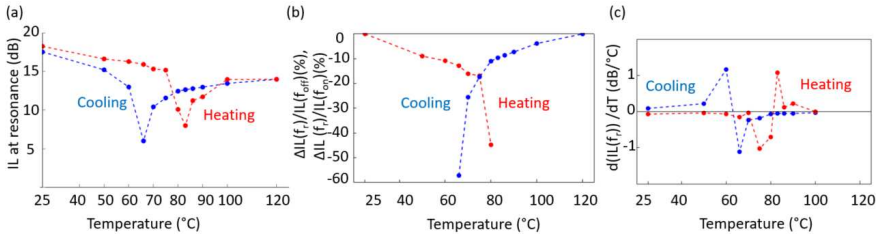

FIG. 5 In heating up and cooling down (a) IL variation with temperature (b) fractional IL variation in respect to the on and off resonance frequencies IL, (c) Derivatives of the IL at resonance frequencies variation in respect to temperature variation.

Finally, Fig. 6 (a) displays the conductivity increase and decrease rate with temperature of the VO_2 DC film, while Fig. 6 (b) shows two variation factors (F_{off} and F_{on}) defined as the fractional variation of resonance frequency in respect to the off/on state ones multiplied with the fractional variation of the maximum attenuation at resonance frequency in respect to the off /on states in heating and cooling (1)

$$F_{off/on} = \frac{\Delta IL(f_r)}{IL(f_{off/on})} * \frac{\Delta(f)}{f_{off/on}} \quad (1)$$

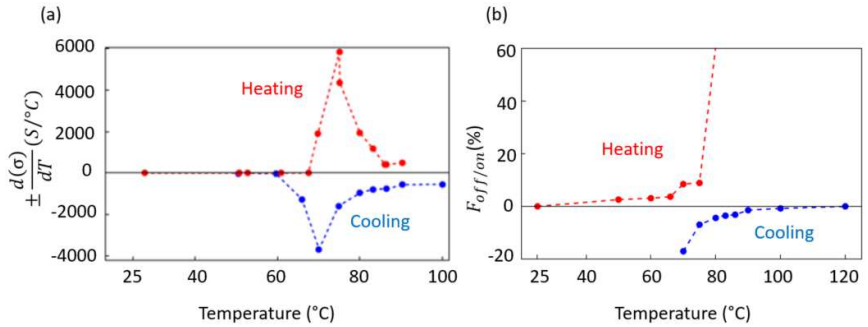

FIG. 6 (a) conductivity increase/decrease rate (b) $F_{off/on}$ variation with temperature in heating-up and cooling-down measurements.

Last, we would like to point out that the measured RF parameters may have completely different responses in heating and cooling also when the temperature is above the T_{ITM} of the VO_2 thin film. Authors (as us too[26, 29-30]) tend to present the results of the reconfigurable RF components in the off state around room temperature and in on state, usually at a single temperature above T_{ITM}[5, 12, 25-30,35] in heating. The behavior of the RF devices at other temperatures is seldom checked, with few exceptions in discrete frequency points[16] in heating and cooling, while on a broadband frequency range but only in heating-up from room temperature to 80 °C[36], Table 2 showing briefly the RF devices testing tendency in literature, compared with this work. Fig. 7 illustrates the discrepancy of the measured filter S21 parameters at 80 °C in cooling down from 120 °C and heating-up from room temperature to 80 °C above T_{ITM} of the thin film which is around 71 °C.

Table II. RF VO_2 based reconfigurable components testing temperatures in heating-up and or cooling-down.

References	Temperatures	heating	cooling	Comment
5	27 °C/68 °C	yes	-	Simulation, 2 temperatures, off/on, one of the first works in RF
12	below 68 °C/above 68 °C	yes	-	2 temperatures, off/on
15	below 68 °C/above 68 °C	yes	-	2 temperatures, off/on, we refer to the results presented in the article overlapping the RF band in between 100 GHz-300 GHz
16	30 °C - 90 °C	yes	yes	in discrete frequency points the RF switches are tested at more temperatures
25	21 °C/90 °C	yes	yes	2 temperatures, off/on
26, 29, 30	25 °C/100 °C	yes	-	2 temperatures, off/on, us in previous works
27	Room temperature/80 °C	yes	-	2 temperatures, off/on
35	Room temperature/85 °C	yes		2 temperatures, off/on
36	20 °C-80 °C	yes	-	Measured in heating
this work	25 °C-120 °C	yes	yes	Measured in 12 different temperature points, history of the device influences its S parameters measurement, especially close to the VO_2 thin film transition temperature (Fig.7)

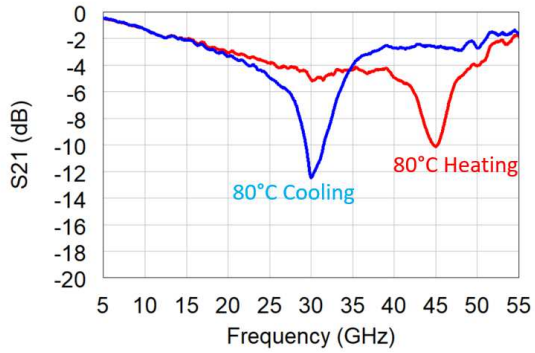

FIG. 7 Heating-up and cooling-down the filter: measurement for the S21 parameters above the T_{ITM} of the VO_2 thin film at 80 °C- dB plot.

In conclusion, we have studied and discussed the RF performances temperature dependencies for a reconfigurable bandstop filter using VO_2, showing unique behavior specific to this class of phase change materials. Further, we report thermal sensitivity and stability analysis of the RF filters with VO_2 switches below the transition temperature and above. It was seen that while the resonance frequency of the filters follows the sharp transition of the VO_2 DC film conductivity characteristics, not the same is the case in the terms of bandstop rejection, which is very much affected by each conductivity level change. Moreover, we have noticed that in order to keep the fractional resonance frequency variation below 1 % one can increase in the off state the temperature to up to 75°C, then a sharp shift of 34% is observed. Similar results were observed for the off state, these results conclude that although temperature stability is very important for keeping high bandstop rejection levels, not the same is the case for the resonance frequencies. Last we have found that in the case of VO_2 RF filters, an accurate predictive modeling of RF performance needs to include the temperature history of the RF

device in case the transition temperature is crossed, or to maintain the temperature considerably above their T_{ITM}, or considerably below their T_{MIT}.

ACKNOWLEDGEMENTS

This work was supported by the HORIZON 2020 FET OPEN PHASE-CHANGE SWITCH Project under Grant 737109. Andrei Muller would also like to ack. Riyaz A. Khadar for the very kind and decisive help in the fabrication flow.

Data Availability Statement

The data that support the findings of this study are available from the corresponding author upon reasonable request.

REFERENCES

[1] 1 F. J. Morin, Phys. Rev. Lett. 3, 34 (1959).

[2] J. B. Goodenough, J. Solid State Chem. 3, 490 (1971)

[3] R. Shi, N. Shen, J. Wang, W. Wang, A. Amini, N. Wang, and C. Cheng, Appl. Phys. Rev. **6**, 011312 (2019).

[4] A. Cavalleri, T. Dekorsy, H.H.W. Chong, J.C. Kieffer, and R.W. Schoenlein, Physical Review B **70**, (2004).

[5] M. Dragoman, A. Cismaru, H. Hartnagel, and R. Plana, Applied Physics Letters **88**, 073503 (2006).

[6] N.F. Quackenbush, J.W. Tashman, J.A. Mundy, S. Sallis, H. Paik, R. Misra, J.A. Moyer, J.-H. Guo, D.A. Fischer, J.C. Woicik, D.A. Muller, D.G. Schlom, and L.F.J. Piper, Nano Letters **13**, 4857 (2013).

[7]G. J. Kovacs, D. Burger, I. Skorupa, H. Reuther, R. Heller, and H. Schmidt, J. Appl. Phys. 109, 063708 (2011)

[8]A. Krammer, A. Magrez, W.A. Vitale, P. Mocny, P. Jeanneret, E. Guibert, H.J. Whitlow, A.M. Ionescu, and A. Schüler, Journal of Applied Physics **122**, 045304 (2017).

[9] T. Driscoll, S. Palit, M.M. Qazilbash, M. Brehm, F. Keilmann, B.-G. Chae, S.-J. Yun, H.-T. Kim, S.Y. Cho, N.M. Jokerst, D.R. Smith, and D.N. Basov, Applied Physics Letters **93**, 024101 (2008).

[10] H. Kocer, S. Butun, B. Banar, K. Wang, S. Tongay, J. Wu, and K. Aydin, Applied Physics Letters **106**, 161104 (2015).

[11] K. Nishikawa, K. Yatsugi, Y. Kishida, and K. Ito, Applied Physics Letters **114**, 211104 (2019).

[12] V. Sanphuang, N. Ghalichechian, N.K. Nahar, and J.L. Volakis, Applied Physics Letters **107**, 253106 (2015).

[13]V. Sanphuang, N. Ghalichechian, N.K. Nahar, and J.L. Volakis, IEEE Transactions on Terahertz Science and Technology **6**, 583 (2016).

[14] H.-F. Zhu, L.-H. Du, J. Li, Q.-W. Shi, B. Peng, Z.-R. Li, W.-X. Huang, and L.-G. Zhu, Applied Physics Letters **112**, 081103 (2018).

[15] A. Chen and Z. Song, IEEE Transactions on Nanotechnology **19**, 197 (2020).

[16]J. Lee, D. Lee, S.J. Cho, J.-H. Seo, D. Liu, C.-B. Eom, and Z. Ma, Applied Physics Letters **111**, 063110 (2017).

[17]P. Grant, M. Denhoff, and R. Mansour, 2004 International Conference on MEMS, NANO and Smart Systems (ICMENS04).

[18]S. Yang, C. Zhang, H.K. Pan, A.E. Fathy, and V.K. Nair, IEEE Microwave Magazine 10, 66 (2009).

[19]Y. Yashchyshyn, K. Derzakowski, G. Bogdan, K. Godziszewski, D. Nyzovets, C.H. Kim, and B. Park, IEEE Antennas and Wireless Propagation Letters 17, 225 (2018).

[20]Y. Gong, J.W. Teng, and J.D. Cressler, 2019 IEEE Radio Frequency Integrated Circuits Symposium (RFIC) (2019).

[21]G. Rebeiz and J. Muldavin, IEEE Microwave Magazine 2, 59 (2001).

[22]L. Katehi, J. Harvey, and E. Brown, IEEE Transactions on Microwave Theory and Techniques 50, 858 (2002).

[23]J. Pal, Y. Zhu, B. Wang, J. Lu, F. Khan, D.V. Dao, and Y. Wang, Applied Physics Letters 108, 253501 (2016).

[24]L.-Y. Ma, N. Soin, M.H.M. Daut, and S.F.W.M. Hatta, IEEE Access 7, 107506 (2019).

[25]D.E. Anagnostou, D. Torres, T.S. Teeslink, and N. Sepulveda, IEEE Antennas and Propagation Magazine **62**, 58 (2020).

[26]A.A. Muller, A. Moldoveanu, V. Asavei, R.A. Khadar, E. Sanabria-Codesal, A. Krammer, M. Fernandez-Bolaños, M. Cavalieri, J. Zhang, E. Casu, A. Schuler, and A.M. Ionescu, Scientific Reports **9**, (2019).

[27]W.A. Vitale, L. Petit, C.F. Moldovan, M. Fernández-Bolaños, A. Paone, A. Schüler, and A.M. Ionescu, Sensors and Actuators A: Physical **241**, 245 (2016).

[28]M. Agaty, A. Crunteanu, C. Dalmay, and P. Blondy, 2018 48th European Microwave Conference (EuMC) (2018).

[29]E.A. Casu, A.A. Muller, M. Fernandez-Bolanos, A. Fumarola, A. Krammer, A. Schuler, and A.M. Ionescu, IEEE Access **6**, 12206 (2018).

[30]A.A. Muller, R.A. Khadar, E.A. Casu, A. Krammer, M. Cavalieri, A. Schuler, J. Zhang, and A.M. Ionescu, 2019 IEEE MTT-S International Microwave Symposium (IMS) (2019).

[31]B. Rong, J. Burghartz, L. Nanver, B. Rejaei, and M. Vanderzwan, IEEE Electron Device Letters 25, 176 (2004).

[32]M. Fernández-Bolaños, J. Perruisseau-Carrier, P. Dainesi, and A. Ionescu, Microelectronic Engineering 85, 1039 (2008).

[33] B. Chen, V.N. Sekhar, C. Jin, Y.Y. Lim, J.S. Toh, S. Fernando, and J. Sharma, IEEE Transactions on Components, Packaging and Manufacturing Technology 3, 1443 (2013).

[34]O. Sydoruk, E. Tatartschuk, E. Shamonina, and L. Solymar, Journal of Applied Physics 105, 014903 (2009).

[35]A. Shamim, M. Vaseem, A. Sizhe, and M.F. Farooqui, 2018 International Flexible Electronics Technology Conference (IFETC) (2018).

[36]E. Shin, K. Pan, W. Wang, G. Subramanyam, V. Vasilyev, K. Leedy, and T. Quach, Materials Research Bulletin 101, 287 (2018).

AIP Publishing

Applied Physics Letters ACCEPTED MANUSCRIPT

This is the author's peer reviewed, accepted manuscript. However, the online version of record will be different from this version once it has been copyedited and typeset.

PLEASE CITE THIS ARTICLE AS DOI: 10.1063/5.0021942

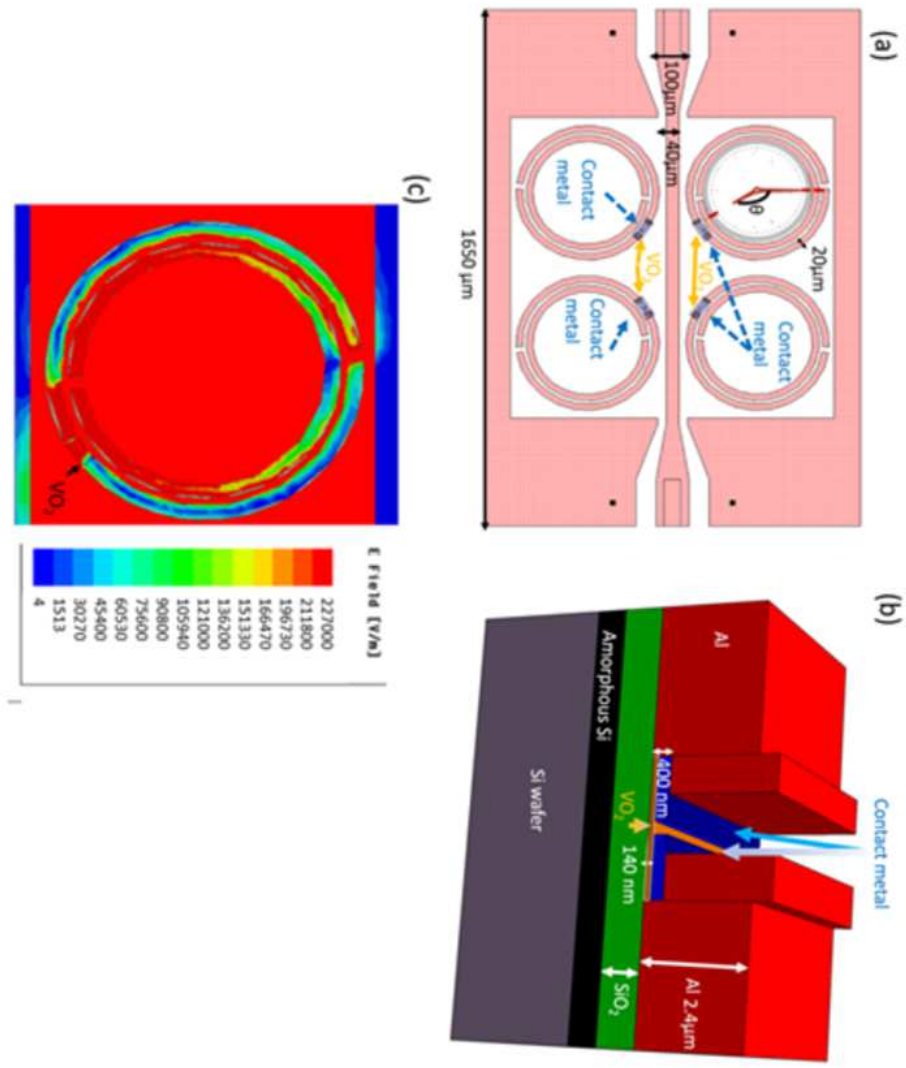

PLEASE CITE THIS ARTICLE AS DOI: 10.1063/5.0021942

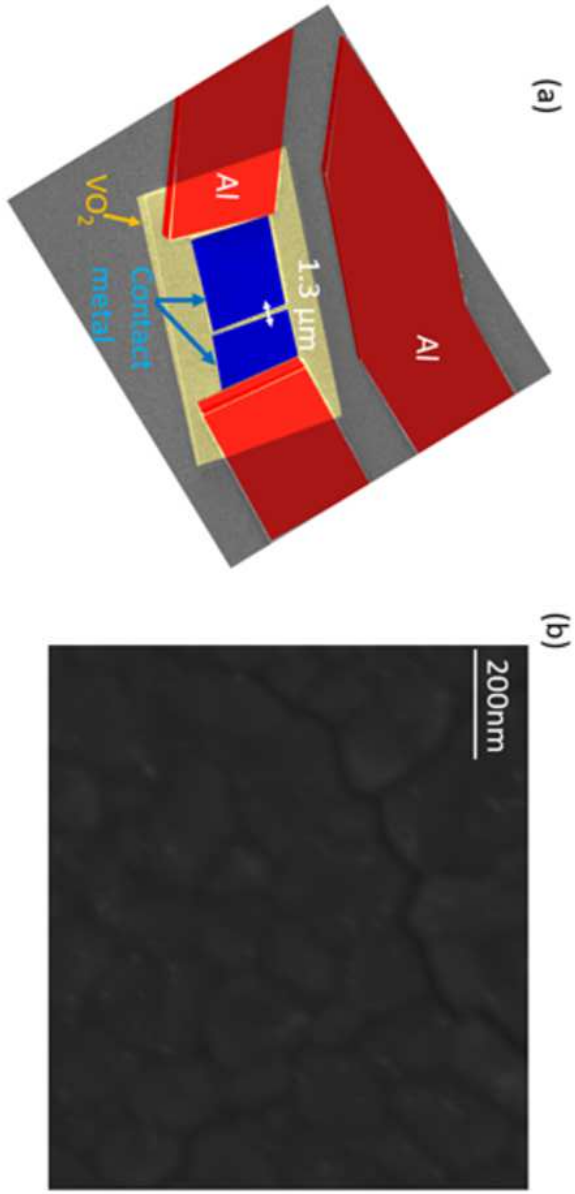

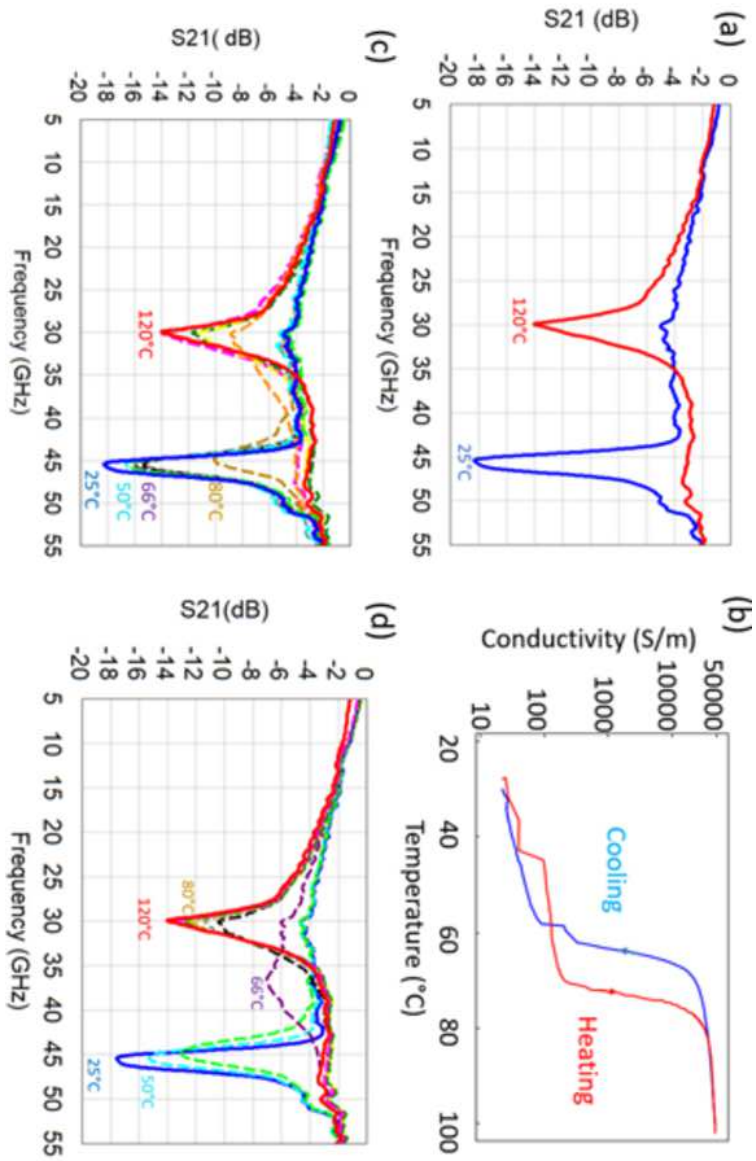

PLEASE CITE THIS ARTICLE AS DOI: 10.1063/5.0021942

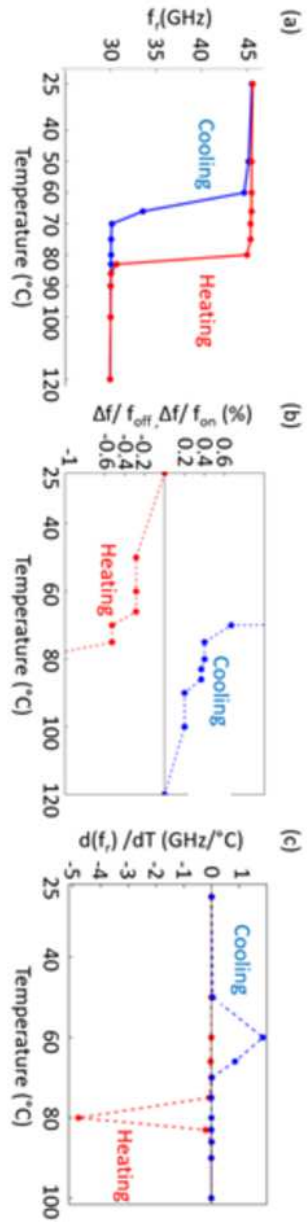

PLEASE CITE THIS ARTICLE AS DOI: 10.1063/5.0021942

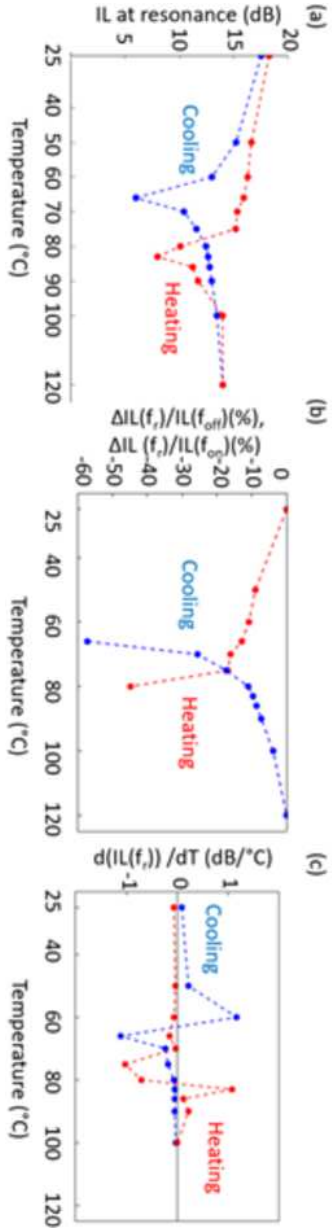

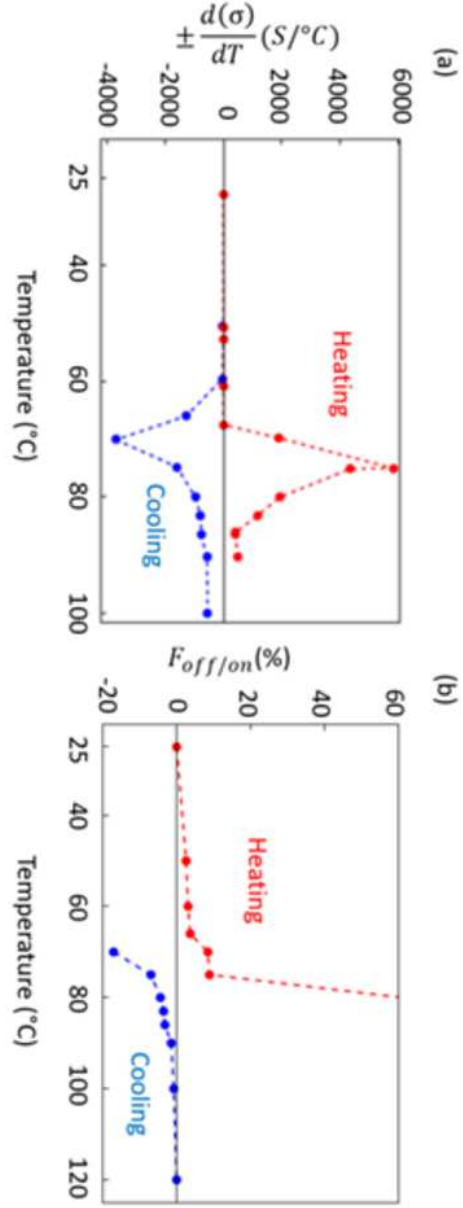

PLEASE CITE THIS ARTICLE AS DOI: 10.1063/5.0021942